

Predicting Topographic Disease Progression and Treatment Response of Pegcetacoplan in Geographic Atrophy Quantified by Deep Learning

Wolf-Dieter Vogl, PhD, Sophie Riedl, MD, Julia Mai, MD, Gregor S. Reiter, MD, PhD, Dmitrii Lachinov, MSc, Hrvoje Bogunović, PhD, Ursula Schmidt-Erfurth, MD

Purpose: To identify disease activity and effects of intravitreal pegcetacoplan treatment on the topographic progression of geographic atrophy (GA) secondary to age-related macular degeneration quantified in spectral-domain OCT (SD-OCT) by automated deep learning assessment.

Design: Retrospective analysis of a phase II clinical trial study evaluating pegcetacoplan in GA patients (FILLY, NCT02503332).

Subjects: SD-OCT scans of 57 eyes with monthly treatment, 46 eyes with every-other-month (EOM) treatment, and 53 eyes with sham injection from baseline and 12-month follow-ups were included, in a total of 312 scans.

Methods: Retinal pigment epithelium loss, photoreceptor (PR) integrity, and hyperreflective foci (HRF) were automatically segmented using validated deep learning algorithms. Local progression rate (LPR) was determined from a growth model measuring the local expansion of GA margins between baseline and 1 year. For each individual margin point, the eccentricity to the foveal center, the progression direction, mean PR thickness, and HRF concentration in the junctional zone were computed. Mean LPR in disease activity and treatment effect conditioned on these properties were estimated by spatial generalized additive mixed-effect models.

Main Outcome Measures: LPR of GA, PR thickness, and HRF concentration in μm .

Results: A total of 31,527 local GA margin locations were analyzed. LPR was higher for areas with low eccentricity to the fovea, thinner PR layer thickness, or higher HRF concentration in the GA junctional zone. When controlling for topographic and structural risk factors, we report on average a significantly lower LPR by -28.0% (95% confidence interval [CI], -42.8 to -9.4 ; $P = 0.0051$) and -23.9% (95% CI, -40.2 to -3.0 ; $P = 0.027$) for monthly and EOM-treated eyes, respectively, compared with sham.

Conclusions: Assessing GA progression on a topographic level is essential to capture the pathognomonic heterogeneity in individual lesion growth and therapeutic response. Pegcetacoplan-treated eyes showed a significantly slower GA lesion progression rate compared with sham, and an even slower growth rate toward the fovea. This study may help to identify patient cohorts with faster progressing lesions, in which pegcetacoplan treatment would be particularly beneficial. Automated artificial intelligence-based tools will provide reliable guidance for the management of GA in clinical practice. *Ophthalmology Retina* 2023;7:4-13 © 2022 by the American Academy of Ophthalmology. This is an open access article under the CC BY-NC-ND license (<http://creativecommons.org/licenses/by-nc-nd/4.0/>).

 Supplemental material available at www.opthalmologyretina.org.

 See Editorial on page 1.

Geographic atrophy (GA) secondary to nonneovascular age-related macular degeneration (AMD) is a chronic progressive degeneration of the neurosensory macula, threatening vision and leading ultimately to irreversible blindness.¹ Approximately 5 million people worldwide are affected by the disease, characterized by the loss of photoreceptors (PRs), retinal pigment epithelium (RPE), and choriocapillaris.²⁻⁴ As the GA lesions start outside the fovea and relentlessly expand toward the fovea over time,

severe vision loss occurs as soon as the fovea is involved.⁵ Furthermore, GA is considered a bilateral disease, as half of the patients with unilateral GA progress to bilateral GA within 7 years.⁶ Up to now, there is no approved therapy available to slow or halt GA progression and thereby preserve vision.⁷ However, several phase II and III clinical trials are investigating therapeutic approaches to reduce disease progression.⁷ Recently, success has been shown by an intravitreal complement C3 inhibition.⁸ The

randomized, multicenter, single-masked, sham injection—controlled phase II trial (FILLY trial [[ClinicalTrials.gov](https://clinicaltrials.gov/ct2/show/study/NCT02503332), identifier CTgov: NCT02503332]) demonstrated significantly reduced GA lesion growth on fundus autofluorescence (FAF) by intravitreal injection of pegcetacoplan compared with sham treatment in GA secondary to AMD.⁹ These results led to 2 subsequent phase III trials to evaluate the efficacy and safety of intravitreal pegcetacoplan (DERBY: NCT03525600; and OAKS: NCT03525613).

GA progresses slowly and kinetics has been shown to be highly variable between individual patients and even at the level of an individual GA lesion.^{10,11} GA progression rate has been associated with lesion shape (area, number, circularity), direction (toward fovea vs. periphery), topographic locations of PR degeneration, hyperreflective foci (HRF) concentration, junctional zone FAF intensity and patterns, subretinal drusenoid deposits, low-luminance deficit, and surrounding choriocapillaris flow deficits.^{11–24} Commonly, the size of the GA area on FAF has been used for monitoring the progression of atrophy. However, there is a mathematical effect due to the quadratic relationship of area to perimeter that larger lesions at baseline show faster area growth than small lesions, even when GA margin extension progresses with the same constant speed.^{25,26} Furthermore, overall lesion size assessment captures only the global growth, ignoring the dynamic local heterogeneous progression and its relation to local topology and structural characteristics adjacent to the lesion border. Junctional zone and local lesion progression analysis considering the border of GA and its surroundings have been proposed to overcome this limitation of an inadequate evaluation of disease progression.^{10,11,21,25} Local progression is of particular importance, as the integrity or affection of the sensitive fovea is largely responsible for visual maintenance or loss—a major prognostic factor in the management of GA.

In this exploratory post hoc study, we advance the technique of local growth analysis with respect to intravitreal pegcetacoplan treatment. We use the FILLY dataset to broaden the community's insight into the effect of treatment on GA progression at a local level. Furthermore, we model the role of topographic and structural characteristics observed in spectral-domain OCT (SD-OCT) images across the sham and treatment groups. The innovative contribution and clinical relevance of this work are four-fold. (1) We use a fully automated approach to analyze OCT scans and segment (patho)morphologic structures, such as GA lesion extension, PR layer thickness, and HRF in SD-OCT images.^{27–29} (2) We incorporate a framework to compute spatially resolved GA progression kinetics on a local level.²⁴ (3) We correlate local progression rate (LPR) with precise topographic properties, such as GA margin eccentricity toward the foveal center or progression direction, and structural junctional zone properties known to affect GA progression that are PR integrity, and HRF concentration. Furthermore, we relate the local progression kinetics with the specific treatment groups from the FILLY study to respect to topography and retinal structure. (4) We demonstrate the utility of spatial generalized additive mixed-effect models (GAMMs) that allow the modeling of

linear and nonlinear relationships to investigate the correlation of local progression with other relevant factors.

Using our tools, we are able to precisely and reliably capture spatially resolved GA growth and its heterogeneous progression and answer the following questions: (1) Is there a topographic or structural effect that locally amplifies or reduces GA progression? (2) Is the treatment response locally heterogeneous and affected by topographic or structural properties? (3) Does the treatment effect remain significant when correcting for the detected risk factors? This is of particular importance with respect to the lesion growth toward the fovea. Our aim is to introduce automated and reliable artificial intelligence (AI)-based tools allowing an adequate selection of patients who would benefit most from therapy, a quantitative monitoring of therapeutic response over time and to offer a reliable prognosis of visual loss or maintenance in future clinical practice.

Methods

To analyze the local variation in the GA progression rate with respect to spatial and structural features, we developed an image processing and analysis pipeline consisting of 4 major steps: (1) a fully automated segmentation of the GA lesion margins and further biomarkers in SD-OCT volumes at baseline and 1-year follow-up, (2) spatial registration of the 1-year follow-up scan with the baseline scan, (3) a quantification of LPR and biomarkers in the junctional zone of the GA margin, and (4) estimation of the conditional mean GA progression rate on a local level with respect to spatial and structural covariates, as well as the relation to treatment response. In the following sections, the details of the study population and the analysis pipeline are presented.

Study Population

In this study, we used SD-OCT image data from the FILLY trial ([ClinicalTrials.gov](https://clinicaltrials.gov/ct2/show/study/NCT02503332) identifier, NCT02503332), a phase II, prospective, randomized, multicenter, single-masked, sham injection—controlled trial in subjects with GA secondary to non-neovascular AMD. The goal of the trial was to assess the safety, tolerability, and efficacy of intravitreally administered pegcetacoplan. Details about the study design and outcomes have been published.⁹ Briefly, 246 patients were randomized for 15 mg pegcetacoplan intravitreal monthly, 15 mg intravitreal pegcetacoplan every other month (EOM), or sham injection over a period of 12 months and a follow-up of 18 months. The study was conducted in accordance with the tenets of the Declaration of Helsinki. All subjects provided written informed consent. Approval for this post hoc analysis was obtained from the Ethics Committee at the Medical University of Vienna.

The inclusion criterion for this particular study was examination with a Spectralis (Heidelberg Engineering) SD-OCT device both at baseline and at 1 year.

Image Processing and Analysis Pipeline

In the following, we briefly describe the analysis pipeline. A detailed description of the methods and parameter settings are provided in the [Supplemental Materials](#) (available at www.opthalmologyretina.org).

SD-OCT Image Acquisition. As inpatient registration is required for this study, we used scans from the Spectralis OCT (Heidelberg Engineering) that were acquired using the follow-up mode. The imaging protocol for this device was 49 B-scans

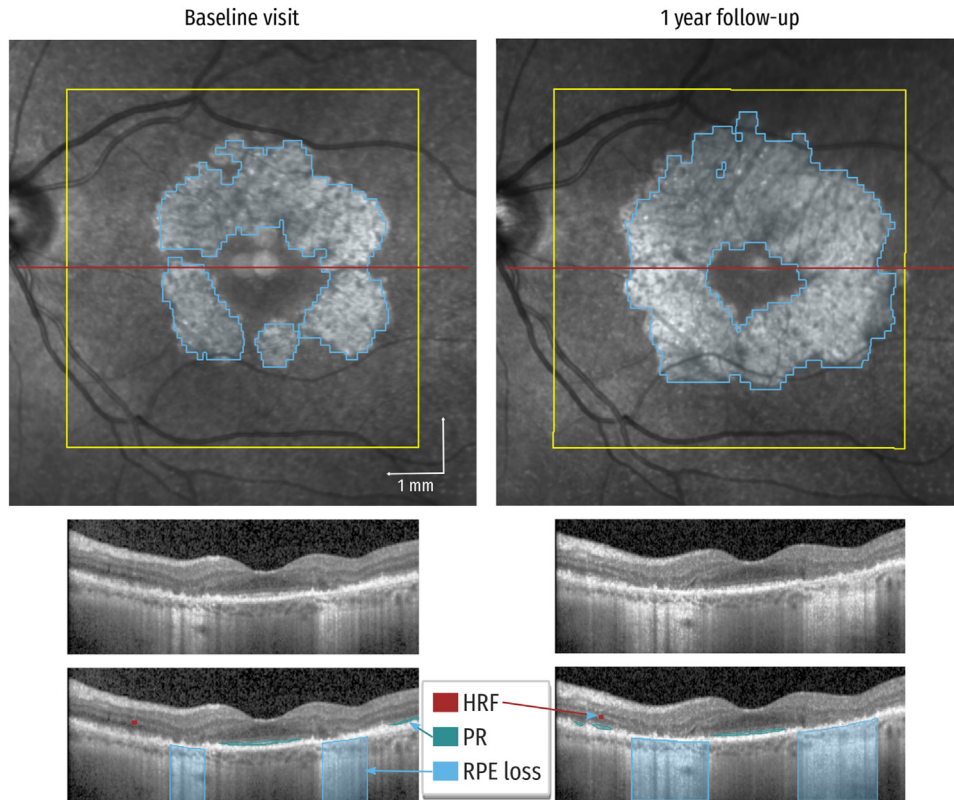


Figure 1. Example from the FILLY study of a monthly treated eye with geographic atrophy (GA) and automatic segmentation of lesion progression. Top: Scanning laser ophthalmoscope image for baseline and 1-year visit with an overlay of automated segmentation of retinal pigment epithelium (RPE) loss (blue) from a SD-OCT image. Bottom: Central B-scan (red line in SLO) with automated segmentations overlaid. Segmentations contain RPE loss (blue), photoreceptor (PR) layer (green), and hyperreflective foci (HRF) and were obtained by deep learning algorithms.

covering the central 20° of the macula. B-scan size is 512×496 with a pixel spacing between and along A-scans of approximately 11 and 3.9 μm , respectively. The distance between B-scan slices was approximately 118 μm .

Segmentation of Structural Features and Computation of En-face Maps. We employed previously validated deep learning models to segment GA lesions, PR layers, and HRF in SD-OCT images, both at baseline and 1-year follow-up (Fig 1).^{27–30} All 3 segmentation algorithms use fully convolutional neural networks with enhanced U-shaped structures to obtain pixel-accurate segmentation of the target structures. GA lesion segmentations use a 3D-to-2D U-Net approach with skip connections to obtain en-face segmentation from a 3D OCT volume. PR layers are segmented between the top of the ellipsoid zone and the inner boundary of the RPE layer per B-scan based on an ensemble of 4 different U-shaped convolutional neural network architectures. With the ensemble approach, individual advantages of each network architecture were incorporated, leading to a more accurate segmentation than with a single-network approach. HRF segmentation was performed per B-scan using a U-Net with residual units (ResU-Net).³¹ To compensate for the different resolutions and pixel spacings in SD-OCT images, all en-face maps were resampled to 512×512 pixels and 15 μm isotropic pixel spacing, which is close to the source A-scan resolution. An isotropic grid is necessary to minimize interpolation errors when performing rigid registration of follow-up scans.

Image Registration of Follow-up Scans. Although in most cases, SD-OCT follow-up volumes were already aligned directly by the scanner software, for 51 cases, this functionality was not

activated during acquisition and follow-up scans did not align with the baseline. Thus, we registered the corresponding scanning laser ophthalmoscope images that were acquired together with the SD-OCT images and used this registration to correctly align all SD-OCT derived from en-face maps.

Quantification of GA LPR. To estimate GA lesion LPR, we used a biophysical growth model framework as described in Moulton et al.²⁴ Briefly, we first determined the GA margin from our automatic GA segmentations (Fig 2A). For each baseline margin point, we developed a growth trajectory to estimate the evolution of the GA margin from baseline to 1-year follow-up within a level-set framework with 2 terms: a constant expansion perpendicular to the GA margin and a curvature term enforcing faster progression for concave margin (Fig 2B). The LPR is then the individual trajectory length in mm. In this framework, merging of GA margins within a lesion or between different lesion foci is intrinsically modeled. Details of the mathematical formulation and parameter settings are provided in the [Supplemental Materials](http://www.ophtalmologyretina.org) (available at www.ophtalmologyretina.org).

We excluded GA margin points that were at the border of an OCT field of view at baseline or where the trajectory ended at the 1-year OCT border, as GA lesions likely progressed beyond the observed area, and thus an exact LPR could not be determined for these sections.

Measuring Structural Properties. In addition to LPR, we determined for each GA margin point the eccentricity to the image center and the direction the lesion margin is facing, either toward the fovea or toward the periphery. The margin eccentricity was determined as the Euclidean distance from each point to the foveal

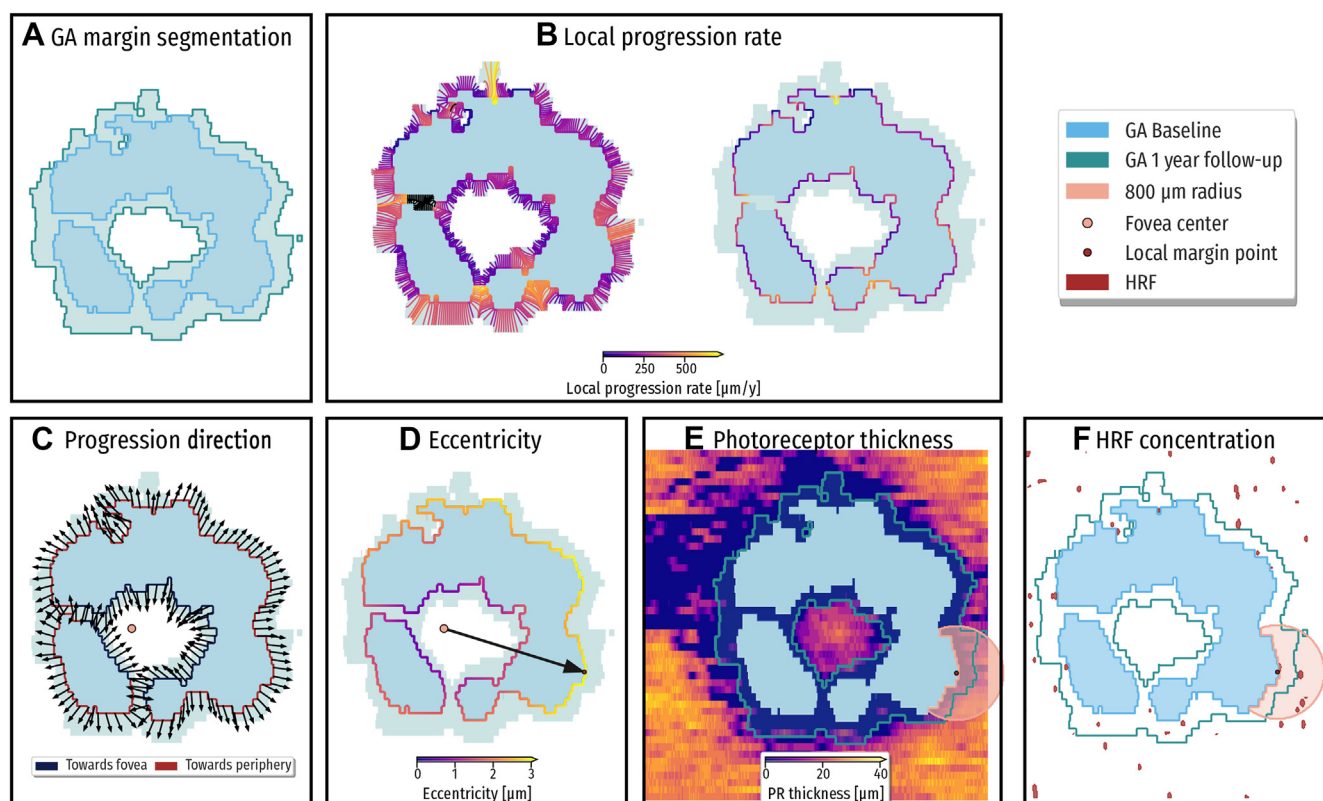


Figure 2. Illustration of the topographic features computed for each baseline geographic atrophy (GA) margin point. The baseline GA area is shown in blue and 1-year progression is shown in green. **A**, Automated segmentation of retinal pigment epithelium (RPE) loss determining GA at baseline and at 1-year. **B**, Local progression rate (LPR) as determined by the level-set growth model. On the left, the individual growth trajectories are illustrated; on the right, the LPR is color coded at each margin point to illustrate local progression activity. **C**, The growth direction toward the fovea (blue margin) or toward the periphery (red margin) is determined from the local tangent normal vector, illustrated here as black arrows. **D**, For each GA margin point, the distance to the fovea is computed. **E**, For each GA margin point, the mean photoreceptor (PR) thickness in the junctional zone (exemplarily demonstrated as the orange circle with 800 μm radius) is computed. **F**, For each GA margin point, the hyperreflective foci (HRF) concentration is computed. Red dots in **F** mark locations of HRF in the retina.

center (Fig 2D). To obtain the direction of growth, we determined the angle between the perpendicular vector of the local GA margin and the vector pointing toward the foveal center. For an angle of less than 180° we defined progression toward the fovea or progression toward the periphery otherwise (Fig 2C).

Measuring the Structural Properties of the Junctional Zone. In addition to topographic features, we computed structural features in proximity to each margin point. Accordingly, we defined a circular junctional zone with a previously established radius of 800 μm centered at each margin point, and computed the aggregation measures of the nonatrophic area.¹⁸ In particular, the mean PR thickness was computed (Fig 2E) within this zone. Furthermore, the HRF concentration was computed as the ratio of total HRF volume in the junctional zone to the junctional zone in the nonatrophic area.¹⁸

Statistical Analysis of Topographic Properties and Treatment Effect on LPR

To assess the relationship of LPR, topographic features, and structural features, and whether they differ among the treatment groups, we first extracted GA features at margin points equally distributed along the contour with a distance of 105 μm (7 pixels) between (in arc length) for each eye: LPR, margin direction and

eccentricity, mean PR thickness, and HRF concentration. The pooled measurements of all study eyes were then analyzed using several generalized linear mixed models (GLMMs) and GAMMs with LPR as the target variable.^{32,33} Subsampling along the contour was necessary for computationally feasible inferencing. The GLMM regression models a linear relationship between LPR and other covariates, and due to its linearity, also enables a straightforward interpretation of the model parameters and *P* values. However, GAMMs that are closely related to the generalized additive model is able to model more complex relationships of LPR and other covariates by introducing smooth spline structures.³³ Whereas the interpretation of coefficients is not as simple as in linear models, explainability can be achieved to some degree, i.e., by plotting the LPR model estimate conditioned on covariate of interest (e.g. conditioned on PR thickness between 0 and 50 μm).

For LPR, we assumed a compound Poisson-gamma distribution,³² where distribution parameters were determined from the data. We accounted for spatial correlation of neighboring margin points in all our models by incorporating a spatial autocorrelation structure with exponential decay.³⁴ Ignoring autocorrelation may lead to a bias by underestimating standard errors, resulting in overly optimistic estimates of the models' predictive ability.³⁵ To account for the general within-subject correlation, we included a grouping of random intercepts per subject in our GLMMs and

Table 1. Patient and GA Lesion Characteristics

	Monthly	EOM	Sham	Total
n	57	46	53	156
Age, yrs, mean \pm SD	79.5 \pm 7.7	79.5 \pm 7.6	77.1 \pm 7.4	78.7 \pm 7.6
Gender, female, no. (%)	37 (64.9%)	28 (60.9%)	35 (66.0%)	100 (64.1%)
Baseline GA lesion size, mean \pm SD (mm ²)	7.25 \pm 3.43	8.07 \pm 4.06	7.92 \pm 3.90	7.72 \pm 3.78
1 year GA lesion size, mean \pm SD (mm ²)	8.62 \pm 3.56	9.81 \pm 4.45	9.87 \pm 4.48	9.40 \pm 4.17
Central GA,* no. (%)	39 (68.4%)	25 (54.3%)	35 (64.8%)	99 (63.5%)

EOM = every other month; GA = geographic atrophy; SD = standard deviation.

GA measurements are quantified from SD-OCT by artificial intelligence-generated segmentations

*Central GA is defined as the presence of GA within a central 1-mm diameter.

GAMMs. Details of the model assumptions and parameters are provided in the [Supplemental Materials](#) available at www.opthalmologyretina.org.

Model Inference. Univariable GLMMs were used to assess the relationship between LPR and the potential risk factors of age, gender, baseline GA area, and treatment. The effects of structural and topographic properties were evaluated with adjustment for treatment in a multivariable GLMM. Furthermore, GAMMs were used to model the nonlinear relationship of eccentricity and photoreceptor thickness with splines. For easier interpretation of the eccentricity and to obtain *P* values, we computed a GLMM model with step-wise distance intervals based on the early treatment diabetic retinopathy study grid (0–0.5, 0.5–1.5, 1.5–3 and > 3 mm). Finally, a multivariable model was computed including all potential risk factors identified in the other analyses.

P values were derived from a t-distribution and the significance level was set to *P* < 0.05. Standard error was used to compute 95% pointwise confidence intervals for the GAMM splines.

Results

Patient Characteristics

In the subset of FILLY, 156 study eyes were eligible for analysis, of which 57, 46, and 53 patients received monthly, EOM, or sham treatment, respectively. Ten study eyes were removed after manual inspection, where SD-OCT and corresponding scanning laser ophthalmoscope image were not accurately aligned by the device, and thus the alignment of baseline and follow-up values was erroneous. Patient characteristics are provided in [Table 1](#).

Evaluation of Key Baseline Characteristics and Overall Treatment Effect

No specific trends in LPR were observed for age, sex, or baseline lesion size, as summarized in [Table 2](#). In this baseline characteristic model, the sham group had a mean LPR of 87.6 μ m (95% CI, 74.2–103.5). The LPR for the pegcetacoplan-treated monthly group was significantly lower by an average of –21.6% (95% CI, –37.9 to –1.1; *P* = 0.04), and lower for EOM treatment by –15.9% (95% CI, –34.2 to 7.5; *P* = 0.17), not reaching significance. [Figure 3](#) shows the distribution of LPR for the 3 treatment groups. Monthly treated eyes had a higher proportion of zero LPR compared with sham-treated eyes, which have more GA boundary locations with LPR > 200 μ m. This result conclusively supports the results reported for the primary results of the FILLY study, however, based on a distinct and realistic resolution of the

individual growth patterns of the GA lesions by an automated AI modality.

Relationship between Local Progression Rate and Treatment with Topographic Characteristics

The Eccentricity and Progression Direction. Illustrating the GAMM fit for LPR versus eccentricity and grouped by progression direction ([Fig 4](#)), we observed a slower progression at larger eccentricities. For cases progressing toward the fovea, we also see a slower progression at close proximity to the fovea and a peaking progression rate at 1-mm eccentricity. Monthly treated eyes showed the slowest progression rate for all eccentricities compared with sham.

To obtain *P* values for comparisons of treatment, and for easier interpretation, we included a linear model with stepwise distances based on the early treatment diabetic retinopathy study grid. As a reference, we used an interval of 0.5–1.5 mm and compared for significant differences in LPR for other ranges. We purposely did not choose the central 0.5 mm as the reference due to the much lower numbers of samples in that interval (see the distribution of samples in [Fig S1](#), available at www.opthalmologyretina.org).

All numbers of the stepwise model are listed in [Table 3](#) for the sham arm, i.e., the natural disease activity and the treatment arms. In the reference interval (0.5–1.5 mm) we observed average progression of 0.105 mm (95% CI, 0.082–0.135) and 0.099 mm (95% CI, 0.083–0.118) toward fovea and periphery, respectively. The difference in progression speed between the central and peripheral locations was significant (*P* = 0.014). Similar to the GAMM, we observed significantly slower

Table 2. Estimated Relative Effect on the LPR in Percentage for Every 1-Unit Increase in Age and Baseline GA Lesion Size and for Male Compared with Female

Characteristic (unit)	Estimate (%)	95% CI	<i>P</i> Value
Age (yrs)	–1.2	–2.5 to 0.1	0.071
Sex (male)	–10.8	–27.5 to 9.7	0.28
Baseline GA lesion size (μ m ²)	–1.4	–3.9 to 1.2	0.30

CI = confidence interval; GA = geographic atrophy; LPR = local progression rate.

Values are obtained from a generalized additive mixed model (GAMM) regression with stepwise distances

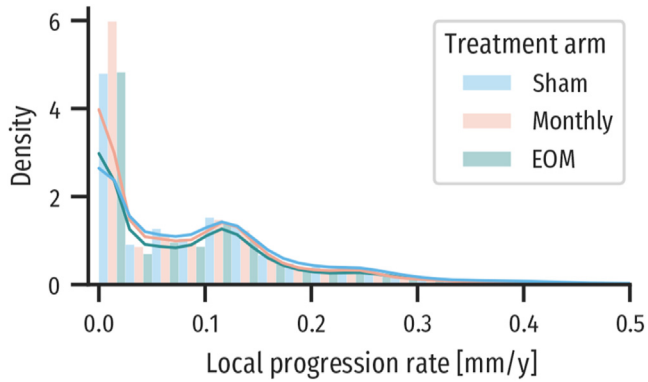


Figure 3. Weighted distribution of local progression rate (LPR) for the 3 treatment arms. Monthly treated eyes have more geographic atrophy (GA) margin locations with low LPR (< 20%). Sham-treated eyes have a higher proportion of moderate and high LPR (> 20%). Every-other-month (EOM) treatment LPR is generally close to sham treatment except in the range of 20%–40%, where it is lower. Distribution is weighted by the reciprocal of GA margin length, to avoid bias by lesions with larger margin area.

progression at larger eccentricity (1.5–3 mm) ($P < 0.01$). Close to the fovea, no significant faster progression toward the foveal center ($P = 0.64$) and trend of faster progression toward the periphery ($P = 0.07$) could be observed.

Regarding treatment, we identified a significant reduction of progression toward the fovea for monthly treated eyes, particularly at close proximity to the fovea. Toward the periphery, the treatment effect showed a trend of being lower than toward the fovea and was only significant for the interval 1.5–3 mm ($P = 0.017$). For EOM-treated eyes, we observed in general a lesser reduction of LPR compared with monthly treatment but no significant effect compared with the sham group. This finding confirms the dose dependency of the therapeutic effect even at the topographic level of a GA lesion.

Photoreceptor Thickness and HRF Concentration. PR thickness in the junctional zone was significantly associated with LPR. GA margin points surrounded by thicker PR showed a slower

progression rate (Fig 5). In the model that controlled for treatment and treatment interaction, we report a change in LPR by -4.3% (95% CI, -5.2 to -3.4 ; $P < 0.0001$) per $1\text{-}\mu\text{m}$ PR thickness, highlighting the ultrastructural precision of an AI-based OCT analysis. Apart from the general treatment effect, we did not observe an additional significantly different treatment effect with respect to PR thickness (monthly, $P = 0.98$; EOM, $P = 0.57$).

Modeling the association of HRF concentration with LPR indicated faster progression associated with a higher HRF concentration in the junctional zone. We observed a change in LPR by $+86.3\%$ (95% CI, $37.7\text{--}152.2$; $P < 0.0001$) per μm of HRF concentration increase in the junctional zone. Be aware that real concentration levels are often small due to the sparse distribution of HRF in the junctional zone. The population mean \pm standard deviation and median (25%, 75% quantile) HRF concentration in the junctional zone are 0.10 ± 0.15 and 0.051 (0.012, 0.123), respectively (see also Fig S2, available at www.opthalmologyretina.org). Thus, for the median case, the average change in LPR is 4.4% (95% CI, $1.9\text{--}7.8$).

Multivariable Analysis with Baseline Structural and Topographic Risk Factors. After controlling the LPR for all previously identified risk factors at baseline (eccentricity curve, progression direction, PR thickness curve, and HRF concentration) in the multivariable GAMM, we observed a significantly lower LPR by -28.0% (95% CI, -42.8 to -9.4 ; $P = 0.0051$) and -23.9% (95% CI, -40.2 to -3.0 ; $P = 0.027$) for monthly and EOM treatments, respectively, compared with sham treatment.

Discussion

GA is a poorly understood and highly underdiagnosed disease in clinical practice. This deficit strongly applies to diagnostic imaging with FAF not routinely available, and although OCT is widely used in AMD management, reliable tools for biomarker assessment are missing. With the advent of novel therapeutic options for this highly prevalent entity, the need for a fast, objective, and quantitative evaluation of disease activity has become a major challenge.

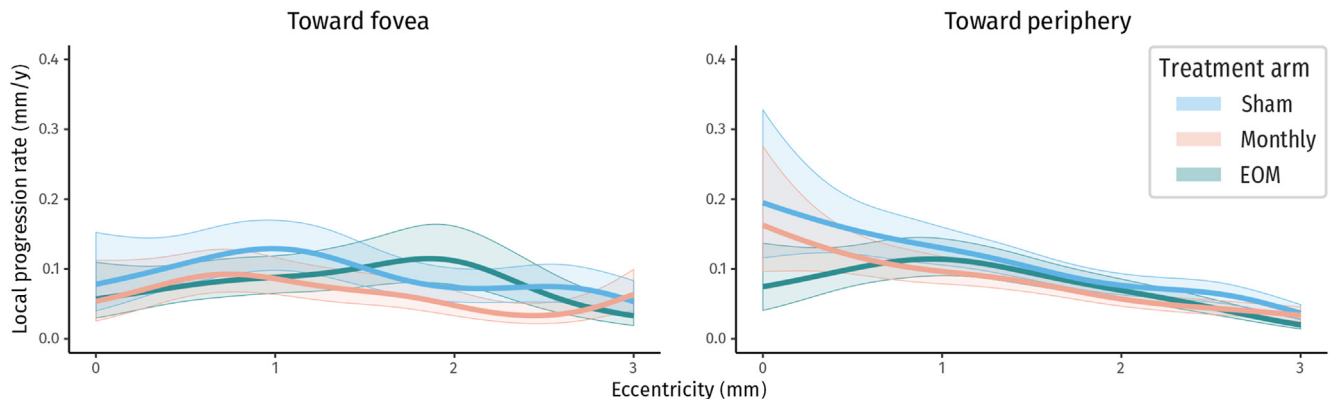


Figure 4. Local progression rate (LPR) with respect to distance to the fovea for locations progressing toward the foveal center (left) and toward the periphery (right) grouped by treatment arms. The marginal mean LPR is approximated by a generalized additive mixed model (GAMM). Bands around mean curves are the 95% confidence intervals (CI). Generally, a slower progression at larger eccentricities is observed. GAMMs also indicate a slower progression toward the fovea at small eccentricities. The treatment effect of monthly treatment consistently shows slower progression over all eccentricities, without a specific regional effect.

Table 3. Estimated Relative Effect on Local Progression Rate Grouped by Progression Direction, the Eccentricity Interval, and Treatment Effect

Characteristic (Eccentricity, Treatment)	Estimate	95% CI	P Value	Estimate	95% CI	P Value
0.5–1.5 mm eccentricity (reference)	0.105 mm	0.082 to 0.135	< 0.0001	0.099 mm	0.083 to 0.118	< 0.0001
Monthly	–32.8%	–53.3 to –3.4	0.032	–21.7%	–38.8 to 0.1	0.051
EOM	–21.3%	–45.4 to 13.5	0.20	–12.7%	–32.8 to 13.2	0.31
0–0.5 mm eccentricity	6%	–16.9 to 35.1	0.64	20.0%	–2.1 to 47.2	0.07
Monthly	–43.6%	–65.2 to –8.8	0.020	–23.5%	–46.9 to 10.2	0.15
EOM	–28.6%	–55.3 to 14.1	0.16	–29.0%	–53.0 to 7.3	0.10
1.5–3 mm eccentricity	–26.9%	–41.8 to –8.3	0.0068	–17.7%	–24.8 to –9.9	< 0.0001
Monthly	–31.5%	–53 to –0.3	0.048	–25.4%	–41.1 to –5.1	0.017
EOM	–4.2%	–34.7 to 40.5	0.82	–18.7%	–36.9 to 4.6	0.11

CI = confidence interval; EOM = every other month.

Relative effects (and corresponding *P* values) show differences in reference within the same level. Thus, eccentricity intervals are compared with 0.5–1.5 mm eccentricity. Within an individual interval, the difference between monthly and EOM treatment to sham in the same interval is estimated. Estimates are obtained from regression analysis using a linear generalized additive mixed model. *P* values indicate the significance level of the relative effect being different from zero, where significance level <0.05 are bold.

The phase II FILLY trial demonstrated an overall slower progression in GA secondary to nonneovascular AMD in patients treated with intravitreal pegcetacoplan, thereby targeting a huge unmet need for reducing the progression of GA, a disease that affects millions of people worldwide, and approximately 1 in 29 individuals over age 75.^{3,9,36} The spectrum in individual disease progression is extensive and prognostic recommendations are difficult, particularly as GA lesions per se demonstrate a variable growth pattern. In this study, we tackled the locally heterogeneous progression of GA lesions by using regular SD-OCT images, in which we segmented and measured (patho) morphologic structures in a fully automated fashion with high precision, using AI-based image analysis. We were able to obtain a precise topographic “heat map” of GA activity around the lesion margins. Furthermore, we correlate the identified features with the GA progression rate under pegcetacoplan treatment using advanced progression modeling and spatial statistics. With this approach, we were able to precisely localize and quantify topographic variations in GA progression, identify morphological and structural properties influencing the progression rate, and correct for these confounding factors to obtain an accurate evaluation of therapeutic efficacy. Our multivariate model suggests that therapy with pegcetacoplan can slow GA progression by a fixed percentage of the nonuniform progression rates. Findings from this model are an essential help to identify patients having a high risk of faster progression particularly toward the fovea and thus also have a larger benefit of treatment. The proposed approach can also serve as a framework for evaluating the efficiency and mechanisms of any upcoming novel GA treatment.

Progression with respect to the distance to the fovea is a key determinant of visual prognosis. Our analyses showed generally slower disease progression at larger eccentricities. This is congruent to prior studies, where the fastest progression was determined within the range of 0.5–1.6 mm and 0.5–1.8 mm for Moulton et al²⁴ and Mauschwitz et al,³⁷ respectively.^{24,37} In our population, we observed a peak in

the progression rate at approximately 1 mm for progression toward the fovea (Fig 4) and a slower progression in the central area. However, when progressing toward the periphery, this peak was not observed, showing faster progression at smaller eccentricity. However, due to the inclusion criteria in the FILLY study, generally larger lesions with fewer margin points are available in close proximity to the fovea, resulting in higher uncertainty of real progression rate in the 0–0.5 mm interval and, furthermore, nonsignificant difference in the progression rate in the 0–1.5 mm interval (Table 3). Compared with our results, Lindner et al¹⁴ reported 2.8× faster progression toward the periphery in terms of square root area progression rate and Moulton et al²⁴ reported approximately 1.9× faster progression, determined from a local growth model. However, these results are not fully comparable with our method, as in our model, eccentricity and progression direction were not treated independently. In terms of treatment effect, on average, a significantly higher reduction in progression toward the fovea versus progression toward the periphery can be observed for monthly treated eyes. The highest reduction was in the central 0.5-mm interval (Table 3). This finding highlights a clinical indication that pegcetacoplan treatment is beneficial in fovea-sparing lesions by slowing the central progression, resulting in extended preservation of central vision.^{5,38}

Importantly, and unique to OCT compared with FAF, we could associate the degree of PR degeneration with future RPE loss, as suggested in the literature.^{21,30,39} Regions with thinner PR or manifest PR atrophy showed on average faster progression. Whereas in Pfau et al³⁹ the association with GA progression was determined only on a global level by using median PR thicknesses at several distances to the GA margin (62 440 and 944 μm), our spatially resolved approach allows accurate determination of the change in local progression with respect to PR thickness in the 800-μm proximity. Also, as the effect of treatment was proportional to the GA progression rate, the treatment effect was more prominent in eyes with thinner PR (Fig 5).

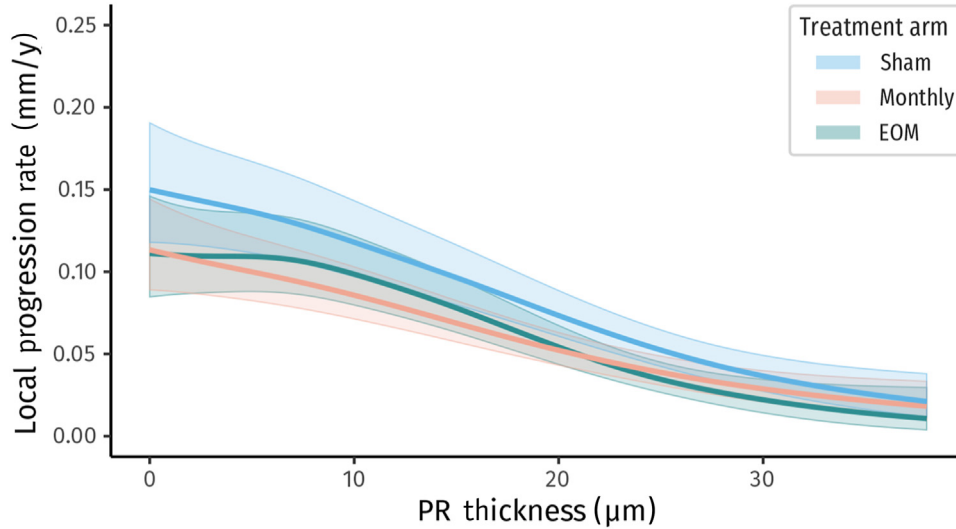


Figure 5. Local progression rate (LPR) with respect to photoreceptor (PR) thickness in the junctional area. The marginal mean LPR is approximated by a generalized additive mixed model (GAMM). Bands around mean curves are the 95% confidence interval (CI). Generally, a faster progression is observed in proximity to thinner PR or PR loss.

Another important biomarker in GA disease is RPE considered as RPE cell migration. Results of this study confirm our previous work, in which presence of HRF was associated with a faster progression rate on a local level.¹⁸ In another data set, mean HRF thickness at the foveal center was lower for eyes progressing to macular atrophy (MA) compared with eyes without disease progression. According to the current findings, at 0.5-mm eccentricity, the largest mean HRF thickness was seen in eyes progressing to MA followed by eyes progressing to idiopathic macular neovascularization and eyes without disease progression.⁴⁰ Topography and the presence of HRF close to the GA margin may already be an indicator of beginning RPE cell death.

By accounting for the above reported confounders, which are topographic properties of the GA margin in terms of eccentricity and progression direction, as well as structural properties in proximity to the GA margin, such as PR thickness and HRF concentration, we were able to show with robust confidence a statistically significant effect of therapy with pegcetacoplan. The standard errors in the treatment effect prediction was reduced when accounting for the risk factors, resulting in a higher statistical power of the model. This finding is of importance for analyzing smaller studies, where an unobserved imbalance in key risk factors between groups may introduce noise and affect the certainty of treatment effect estimation. The estimation of a reduction in LPR by 28% in monthly treatment and the general mean progression rate of around 100 μm is in concordance with the analysis of GA progression on a global level considering the square root transformed GA area change (Note that reported absolute square-root transformed GA area growth rate values as in Steinle et al²² have to be divided by π to obtain an approximation of local progression under the assumption of isotropic growth of a circular lesion¹⁶).^{1,9,22}

Using local progression modeling allowed us to clearly capture the highly nonuniform progression of GA lesions and associate it precisely with local morphologic and

structural properties. In the clinical practice of GA management, this capacity will be key for predicting the natural progression and the therapeutic efficiency for physicians, patients, and payers. The advantage of such an approach in contrast to a global analysis with aggregated features (e.g., median/mean PR thickness within certain distance to GA margin) is that in the latter, the local heterogeneous effects are averaged out, and only strong effects are detectable. However, for a local model, it is of utmost importance to account for spatial autocorrelation, to avoid a significant increase in type I errors (i.e., overoptimistic estimates of models' predictive power)³⁵ due to a reduced degree of freedom of the null distribution. A disadvantage of GAMM in contrast to linear regression models is that interpretation of coefficient values is difficult. Thus, the adjusted marginal mean effect is commonly plotted as a curve (Figs 4, 5) for interpretation. Note that these mean curves are adjusted for autocorrelation effects, which is not the case when naively treating each margin point as an independent sample and computing aggregation values or curve fits from them (e.g., Loess fit) that ultimately results in incorrect estimates of mean effects.

The limitations to our study result mostly from the nature of the original images acquired in the study. First, the spatial resolution is highly anisotropic with a large spacing between B-scan slices in the images available, resulting in a so-called sensor censoring, where small growth less than the distance between 2 B-scans is not observed, and in a general quantization of the progression rate in the direction across B-scans. This effect can also be observed in the histogram in Figure 3, where zero inflation and a local peak at 110 μm is present, which is approximately the concurrent slice distance. To a certain degree, we accounted for the zero-inflation effect by assuming a compound Poisson-gamma distribution that has positive mass at zero. Also, in the growth model framework, we accounted for the staircase effect in the segmented GA margin by introducing a higher

smoothing factor in the initial phase of the interface propagation. There are also caveats in estimating GA progression beyond the perifovea, as the OCT field of view was limited to 20° (approximately 6 × 6 mm). Thus, potentially fast growing areas in the unobserved periphery may have been excluded from the analysis, thereby introducing a downward bias in the progression rate estimate in the perifoveal region. Future studies should consider addressing these issues by acquiring OCT volumes with a smaller distance between B-scans and a larger field of view, which should drive the development of higher-resolution, wider-field OCT devices. Furthermore, the small sample size of around 50 patients per treatment arm limits the ability to discover more subtle effects of features on the outcome, and results in an increased

confidence interval of the effect estimates. Future studies on a larger cohort may provide additional insights and strengthen the findings of this study.

In conclusion, we provided an unprecedented accurate and individualized analysis of spatially resolved GA progression in disease activity and under pegcetacoplan treatment. We were able to plausibly explain highly nonuniform growth by topographic properties that are eccentricity to the fovea, and progression direction, as well as by structural properties, i.e., PR and HRF condition. Such an innovative yet reliable approach is essential for understanding the mechanisms of disease progression and therapeutic intervention, and to optimally guide GA management in the clinical setting.

Footnotes and Disclosures

Originally received: April 5, 2022.

Final revision: July 31, 2022.

Accepted: August 1, 2022.

Available online: August 7, 2022. Manuscript no. ORET-D-22-00234

Department of Ophthalmology, Medical University of Vienna, Austria.

Previously presented at the Annual Meeting of the Association of Research in Vision and Ophthalmology (ARVO) 2021, April 30, 2021, to May 2, 2021: Topographic Effects on AI-Quantified Regional Progression in the FILLY Trial of Pegcetacoplan (APL-2) for the Treatment of Geographic Atrophy Secondary to AMD.

Disclosure(s):

All authors have completed and submitted the ICMJE disclosures form.

The author(s) made the following disclosure(s): U.S.-E.: Scientific consultant – Genentech, Novartis, Roche, Kodiak, and RetInSight.

The FILLY phase II study was conducted by Apellis Pharmaceuticals and our work was supported in part by an Apellis research grant excluding any access to proprietary IP. The financial support by the Austrian Federal Ministry for Digital and Economic Affairs and the National Foundation for Research, Technology and Development is gratefully acknowledged. The funding organizations played no role in the design and conduct of this research.

HUMAN SUBJECTS: Human subjects are included in this study. Informed consent was obtained from all participants. Ethics committee approval was obtained from the Ethics Committee at the Medical University of Vienna. All research adhered to the tenets of the Declaration of Helsinki.

No animals were used in this study.

Author Contributions:

Conception and design: Vogl, Riedl, Mai, Reiter, Bogunović, Schmidt-Erfurth

Data collection: Riedl, Mai, Reiter, Lachinow

Analysis and interpretation: Vogl, Riedl, Mai, Reiter, Bogunović, Schmidt-Erfurth

Obtained funding: Bogunović.

Overall responsibility: Vogl, Riedl, Bogunović, Schmidt-Erfurth

Abbreviations and Acronyms:

AI = artificial intelligence; **AMD** = age-related macular degeneration; **EOM** = every other month; **FAF** = fundus autofluorescence; **GA** = geographic atrophy; **GAMM** = generalized additive mixed-effect model; **GLMM** = generalized linear mixed model; **HRF** = hyperreflective foci; **LPR** = local progression rate; **MA** = macular atrophy; **PR** = photoreceptor; **RPE** = retinal pigment epithelium; **SD** = spectral domain.

Keywords:

Age-related macular degeneration, Deep learning, Geographic atrophy, Image analysis, Optical Coherence tomography.

Correspondence:

Ursula Schmidt-Erfurth, MD, Department of Ophthalmology, Medical University of Vienna, Waehringer Guertel 18-20, Vienna A-1090, Austria. E-mail: ursula.schmidt-erfurth@meduniwien.ac.at.

References

1. Chakravarthy U, Bailey CC, Johnston RL, et al. Characterizing disease burden and progression of geographic atrophy secondary to age-related macular degeneration. *Ophthalmology*. 2018;125:842–849.
2. Rudnicka AR, Jarrar Z, Wormald R, Cook DG, Fletcher A, Owen CG. Age and gender variations in age-related macular degeneration prevalence in populations of European ancestry: a meta-analysis. *Ophthalmology*. 2012;119:571–580.
3. Wong WL, Su X, Li X, et al. Global prevalence of age-related macular degeneration and disease burden projection for 2020 and 2040: a systematic review and meta-analysis. *Lancet Glob Health*. 2014;2:e106–e116.
4. Holz FG, Strauss EC, Schmitz-Valckenberg S, van Lookeren Campagne M. Geographic atrophy: clinical features and potential therapeutic approaches. *Ophthalmology*. 2014;121:1079–1091.
5. Sayegh RG, Sacu S, Dunavölgyi R, et al. Geographic atrophy and foveal-sparing changes related to visual acuity in patients with dry age-related macular degeneration over time. *Am J Ophthalmol*. 2017;179:118–128.
6. Lindblad AS, Lloyd PC, Clemons TE, et al. Change in area of geographic atrophy in the age-related eye disease study: AREDS Report Number 26. *Arch Ophthalmol*. 2009;127:1168–1174.
7. de Guimaraes TAC, Varela MD, Georgiou M, Michaelides M. Treatments for dry age-related macular degeneration: therapeutic avenues, clinical trials and future directions. *Br J Ophthalmol*. 2021;106:297–304.

8. Boyer DS, Schmidt-Erfurth U, van Lookeren Campagne M, et al. The pathophysiology of geographic atrophy secondary to age-related macular degeneration and the complement pathway as a therapeutic target. *Retina*. 2017;37:819–835.
9. Liao DS, Grossi FV, El Mehdi D, et al. Complement C3 inhibitor pegcetacoplan for geographic atrophy secondary to age-related macular degeneration: a randomized phase 2 trial. *Ophthalmology*. 2020;127:186–195.
10. Fleckenstein M, Mitchell P, Freund KB, et al. The progression of geographic atrophy secondary to age-related macular degeneration. *Ophthalmology*. 2018;125:369–390.
11. Moulton EM, Alibhai AY, Lee B, et al. A framework for multiscale quantitation of relationships between choriocapillaris flow impairment and geographic atrophy growth. *Am J Ophthalmol*. 2020;214:172–187.
12. Lindner M, Kosanetzky S, Pfau M, et al. Local progression kinetics of geographic atrophy in age-related macular degeneration are associated with atrophy border morphology. *Invest Ophthalmol Vi Sci*. 2018;59:AMD12–AMD18.
13. Shen LL, Sun M, Ahluwalia A, et al. Geographic atrophy growth is strongly related to lesion perimeter: unifying effects of lesion area, number, and circularity on growth. *Ophthalmology Retina*. 2021;5:868–878.
14. Lindner M, Böker A, Mauschitz MM, et al. Directional kinetics of geographic atrophy progression in age-related macular degeneration with foveal sparing. *Ophthalmology*. 2015;122:1356–1365.
15. Shen LL, Sun M, Khetpal S, et al. Topographic variation of the growth rate of geographic atrophy in nonexudative age-related macular degeneration: a systematic review and meta-analysis. *Invest Ophthalmol Vis Sci*. 2020;61:2, 2.
16. Moulton EM, Hwang Y, Shi Y, et al. Growth modeling for quantitative, spatially resolved geographic atrophy lesion kinetics. *Transl Vis Sci Technol*. 2021;10:26, 26.
17. Reiter GS, Told R, Baumann L, et al. Investigating a growth prediction model in advanced age-related macular degeneration with solitary geographic atrophy using quantitative autofluorescence. *Retina*. 2020;40:1657–1664.
18. Schmidt-Erfurth U, Bogunovic H, Grechenig C, et al. Role of deep learning—quantified hyperreflective foci for the prediction of geographic atrophy progression. *Am J Ophthalmol*. 2020;216:257–270.
19. Bui PTA, Reiter GS, Fabianska M, et al. Fundus autofluorescence and optical coherence tomography biomarkers associated with the progression of geographic atrophy secondary to age-related macular degeneration. *Eye*. 2021:1–7.
20. Marsiglia M, Boddu S, Bearely S, et al. Association between geographic atrophy progression and reticular pseudodrusen in eyes with dry age-related macular degeneration. *Invest Ophthalmol Vis Sci*. 2013;54:7362–7369.
21. Reiter GS, Told R, Schranz M, et al. Subretinal drusenoid deposits and photoreceptor loss detecting global and local progression of geographic atrophy by SD-OCT imaging. *Invest Ophthalmol Vis Sci*. 2020;61:11–11.
22. Steinle NC, Pearce I, Monés J, et al. Impact of baseline characteristics on geographic atrophy progression in the FILLY trial evaluating the complement C3 inhibitor pegcetacoplan. *Am J Ophthalmol*. 2021;227:116–124.
23. Thulliez M, Zhang Q, Shi Y, et al. Correlations between choriocapillaris flow deficits around geographic atrophy and enlargement rates based on swept-source OCT imaging. *Ophthalmology Retina*. 2019;3:478–488.
24. Moulton EM, Shi Y, Zhang Q, et al. Analysis of correlations between local geographic atrophy growth rates and local OCT angiography measured choriocapillaris flow deficits. *Biomed Opt Express*, BOE. 2021;12:4573–4595.
25. Uji A, Nittala MG, Hariri A, et al. Directional kinetics analysis of the progression of geographic atrophy. *Graefes Arch Clin Exp Ophthalmol*. 2019;257:1679–1685.
26. Feuer WJ, Yehoshua Z, Gregori G, et al. Square root transformation of geographic atrophy area measurements to eliminate dependence of growth rates on baseline lesion measurements: a reanalysis of age-related eye disease study report No. 26. *JAMA Ophthalmol*. 2013;131:110–111.
27. Lachinov D, Seeböck P, Mai J, et al. Projective skip-connections for segmentation along a subset of dimensions in retinal OCT. In: de Bruijne M, Cattin PC, Cotin S, et al., eds. *Medical Image Computing and Computer Assisted Intervention – MICCAI 2021 Lecture Notes in Computer Science*. Cham: Springer International Publishing; 2021:431–441.
28. Orlando JI, Gerendas BS, Riedl S, et al. Automated quantification of photoreceptor alteration in macular disease using optical coherence tomography and deep learning. *Sci Rep*. 2020;10:5619.
29. Schlegl T, Bogunovic H, Klimescha S, et al. Fully automated segmentation of hyperreflective foci in optical coherence tomography images. *arXiv*. 2018;1805.03278.
30. Riedl S, Vogl WD, Mai J, et al. The effect of pegcetacoplan treatment on photoreceptor maintenance in geographic atrophy monitored by artificial intelligence–based OCT analysis. *Ophthalmol Retina*. 2022;6(11):1009–1018.
31. Anas EMA, Nouranian S, Mahdavi SS, et al. Clinical target-volume delineation in prostate brachytherapy using residual neural networks. In: Descoteaux M, Maier-Hein L, Franz A, et al., eds. *Medical Image Computing and Computer Assisted Intervention - MICCAI 2017 Lecture Notes in Computer Science*. Cham: Springer International Publishing; 2017:365–373.
32. Dunn PK, Smyth GK. *Generalized Linear Models with Examples in R*. New York, NY: Springer; 2018.
33. Wood SN. *Generalized Additive Models: an Introduction with R*. New York: Chapman and Hall/CRC; 2017.
34. Dormann CF, McPherson JM, Araújo MB, et al. Methods to account for spatial autocorrelation in the analysis of species distributional data: a review. *Ecography*. 2007;30:609–628.
35. Clifford P, Richardson S, Hemon D. Assessing the significance of the correlation between 2 spatial processes. *Biometrics*. 1989;45:123–134.
36. Sunness JS. The natural history of geographic atrophy, the advanced atrophic form of age-related macular degeneration. *Mol Vis*. 1999;5:25.
37. Mauschitz MM, Fonseca S, Chang P, et al. Topography of geographic atrophy in age-related macular degeneration. *Invest Ophthalmol Vis Sci*. 2012;53:4932–4939.
38. Shen LL, Sun M, Ahluwalia A, et al. Natural history of central sparing in geographic atrophy secondary to nonexudative age-related macular degeneration. *Br J Ophthalmol*. 2022;106:689–695.
39. Pfau M, von der Emde L, de Sisternes L, et al. Progression of photoreceptor degeneration in geographic atrophy secondary to age-related macular degeneration. *JAMA Ophthalmol*. 2020;138:1026–1034.
40. Waldstein SM, Vogl WD, Bogunovic H, et al. Characterization of drusen and hyperreflective foci as biomarkers for disease progression in age-related macular degeneration using artificial intelligence in optical coherence tomography. *JAMA Ophthalmol*. 2020;138:740–747.